JCB Article

Tyrosine cross-linking of extracellular matrix is catalyzed by Duox, a multidomain oxidase/peroxidase with homology to the phagocyte oxidase subunit gp91*phox*

William A. Edens,[1] Lisa Sharling,[1] Guangjie Cheng,[1] Raymond Shapira,[1] Joseph M. Kinkade,[1] Taehoon Lee,[1] Heather A. Edens,[2] Xuexin Tang,[2] Cameron Sullards,[1] Denise B. Flaherty,[2] Guy M. Benian,[2] and J. David Lambeth[1]

[1]Department of Biochemistry and [2]Department of Pathology, Emory University Medical School, Atlanta, GA 30322

High molecular weight homologues of gp91*phox,* the superoxide-generating subunit of phagocyte nicotinamide adenine dinucleotide phosphate (NADPH)-oxidase, have been identified in human (h) and *Caenorhabditis elegans* (Ce), and are termed Duox for "dual oxidase" because they have both a peroxidase homology domain and a gp91*phox* domain. A topology model predicts that the enzyme will utilize cytosolic NADPH to generate reactive oxygen, but the function of the ecto peroxidase domain was unknown. Ce-Duox1 is expressed in hypodermal cells underlying the cuticle of larval animals. To investigate function, RNA interference (RNAi) was carried out in *C. elegans*. RNAi animals showed complex phenotypes similar to those described previously in mutations in collagen biosynthesis that are known to affect the cuticle, an extracellular matrix. Electron micrographs showed gross abnormalities in the cuticle of RNAi animals. In cuticle, collagen and other proteins are cross-linked via di- and trityrosine linkages, and these linkages were absent in RNAi animals. The expressed peroxidase domains of both Ce-Duox1 and h-Duox showed peroxidase activity and catalyzed cross-linking of free tyrosine ethyl ester. Thus, Ce-Duox catalyzes the cross-linking of tyrosine residues involved in the stabilization of cuticular extracellular matrix.

Introduction

Reactive oxygen generation is well characterized in phagocytes where the respiratory burst oxidase (termed nicotinamide adenine dinucleotide phosphate [NADPH]*-oxidase) catalyzes NADPH-dependent reduction of molecular oxygen to generate superoxide and secondarily metabolites including hydrogen peroxide (Babior, 1995). In the phagocyte, reactive oxygen generation is robust, and high levels of reactive oxygen species participate in bacterial killing. In recent years, it has become clear that nonphagocytic cells also generate reactive oxygen, albeit at lower levels (Cross and Jones, 1991). The origin and function of this reactive oxygen has not been clear and has been attributed variously to "leaky" mitochondrial respiration, the activity of enzymes such as xanthine oxidase, or to the phagocyte NADPH-oxidase itself. In some cases, the reactive oxygen-generating system has properties reminiscent of the phagocyte oxidase (Emmendorffer et al., 1993; Griendling et al., 1994), but it has often been difficult to demonstrate significant expression of critical phagocyte oxidase components in these cell types (Emmendorffer et al., 1993), suggesting the existence of one or more homologues of the phagocyte NADPH-oxidase.

The phagocyte NADPH-oxidase consists of multiple subunits including gp91*phox*, the catalytic moiety (Babior, 1995; Yu et al., 1998). In activated cells, this subunit is associated with the plasma membrane (or with the phagosomal membrane, which is derived from the plasma membrane)

Address correspondence to J. David Lambeth, Department of Biochemistry, Emory University Medical School, Atlanta, GA 30322. Tel.: (404) 727-5875. Fax: (404) 727-2738. E-mail: dlambe@bimcore.emory.edu

W.A. Edens, L. Sharling, and G. Cheng contributed equally to this work.

T. Lee's present address is National Creative Research Initiatives Center for Calcium and Learning, Pohang University of Science and Technology, 790-784 Pohang, Korea.

*Abbreviations used in this paper: Ce-Duox, *Caenorhabditis elegans* Duox; dsRNA, double-stranded RNA; FAD, flavin adenine dinucleotide; h-Duox, human Duox; MPO, myeloperoxidase; NADPH, nicotinamide adenine dinucleotide phosphate; RACE, rapid amplification of cDNA ends; RNAi, RNA interference; TMB, 3,3′,5,5′-tetramethylbenzidine.

Key words: NADPH-oxidase; peroxidase; extracellular matrix; cuticle; dityrosine

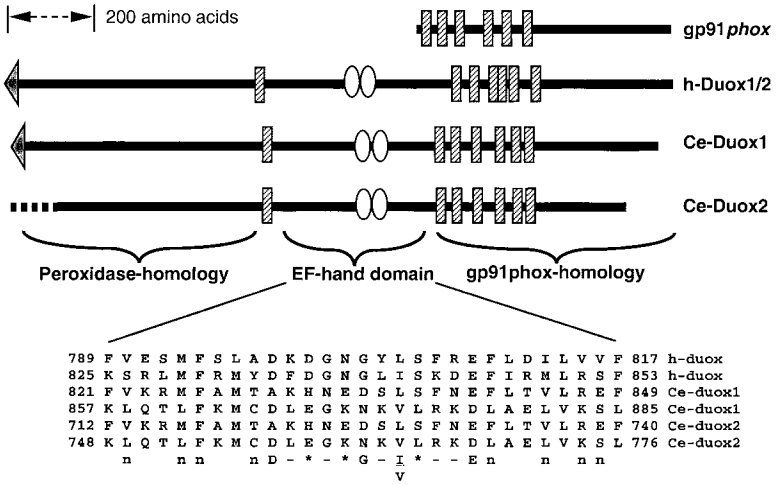

Figure 1. **Structure of large homologues of gp91*phox*.** Domain structure of Duox proteins. Secretory signal peptide sequences are indicated by a gray triangle, whereas predicted transmembrane α helices are indicated by hashed rectangles. White ovals indicate regions showing homology with EF-hand calcium-binding sites.

and consists of a COOH-terminal flavoprotein domain containing the NADPH-binding site (Rotrosen et al., 1992; Segal et al., 1992; Taylor et al., 1993; Takeshige and Sumimoto, 1994) and an NH_2-terminal hydrophobic region comprised of five to six transmembrane α helices and harboring the two heme groups (Cross et al., 1995; Nisimoto et al., 1995; Yu et al., 1998). The structure of the enzyme permits the coupling of the oxidation of intracellular NADPH to the reduction of molecular oxygen to generate extracellular or phagosomal superoxide. Myeloperoxidase (MPO) is secreted extracellularly or into the phagosome, permitting reactive oxygen generated by the phagocyte oxidase to support hypochlorous acid generation in the extracellular/phagosomal compartment (Hampton et al., 1998; Nauseef, 1998).

Based on the hypothesis that reactive oxygen generation in nonphagocytic cells originates in part from homologues of the phagocyte oxidase, we have searched for and molecularly cloned homologues of gp91*phox*. The first of these, Nox1 (also termed Mox1, NOH-1), is expressed in nonphagocytic cells, including colonic epithelia and vascular smooth muscle (Suh et al., 1999), and functions in regulating cell growth and cell transformation. Alternative splicing of Nox1 to generate a portion of the membrane domain produces a proton channel (Banfi et al., 2000) with properties similar to voltage-gated channels. Additional homologues of gp91*phox* that are similar in size to gp91*phox* (~65 kD) have been reported recently (Lambeth et al., 2000; Cheng et al., 2001).

In the present study, we describe large molecular weight homologues of gp91*phox* termed Duox, which are present in human and *C. elegans*. The term Duox, referring to dual oxidase, has been accepted by the Human Genome Organisation International Committee on Gene Nomenclature. A partial sequence of Duox2 was reported recently and termed $p138^{Tox}$, referring to thyroid oxidase. Surprisingly, these homologues contain not only the gp91*phox* homology region at the COOH terminus but also an NH_2-terminal region that is homologous to peroxidases including MPO. Using RNA interference (RNAi) in *C. elegans* to knock out the expression of the nematode Duox1, we find that Duox participates through tyrosine cross-linking in the biogenesis of cuticle, the collagenous extracellular matrix that forms the outer covering of nematodes. The tyrosine cross-linking reaction has also been reconstituted biochemically using the expressed peroxidase domains of human (h)-Duox and *Caenorhabditis elegans* (Ce)-Duox1.

Results

cDNA cloning of human dual oxidases

The cDNA for h-Duox1 was a 4,563 base pair ORF (sequence data available from GenBank/EMBL/DDBJ under accession no. AF213465) that is predicted to encode a protein of 1,521 amino acids (177 kD), nearly three times the size of gp91*phox* (Fig. 1). A consensus Kozak sequence, ATCATGG, was present at the translation start codon. The cDNA for h-Duox2 showed a 4,647 base pair ORF (sequence data available from GenBank/EMBL/DDBJ under accession no. AF267981) that is predicted to encode a protein of 1,548 amino acids (175 kD) and contained a consensus Kozak sequence, GGCATGC, at the translation start codon. The Duox2 cDNA sequence is a larger form of a gp91*phox* homologue identified previously as an NADPH-oxidase in thyroid and termed $p138^{Tox}$; the latter sequence did not contain the peroxidase homology domain (Dupuy et al., 1999). h-Duox1 and h-Duox2 were 77% identical at the amino acid level. These sequences were independently cloned recently and reported by De Deken et al. (2000).

Duox homologues in *C. elegans*

A BLAST search of the *C. elegans* genomic database using as a query the protein sequence of gp91*phox* identified two homologous genes contained in cosmids F56C11 and F53G12. The Ce-Duox1 conceptual transcript (sequence data available from GenBank/EMBL/DDBJ under accession no. AF043697) is predicted to be 8,197 bp before splicing, to contain 19 exons, and to encode a protein of 1,506 amino acids. Cloning of the cDNA for Ce-Duox1 (sequence data available from GenBank/EMBL/DDBJ under accession no. AF229855) revealed a cDNA of 4,491 bp (1,497 amino acids), which differed somewhat from the conceptual cDNA obtained from the gene structure due to inaccuracies in the predicted intron-exon junctions. The second transcript, Ce-Duox2 (sequence data available from GenBank/EMBL/DDBJ under accession no. AF043697), is predicted to be 5,308 bp before splicing, to contain 16 exons, and to encode

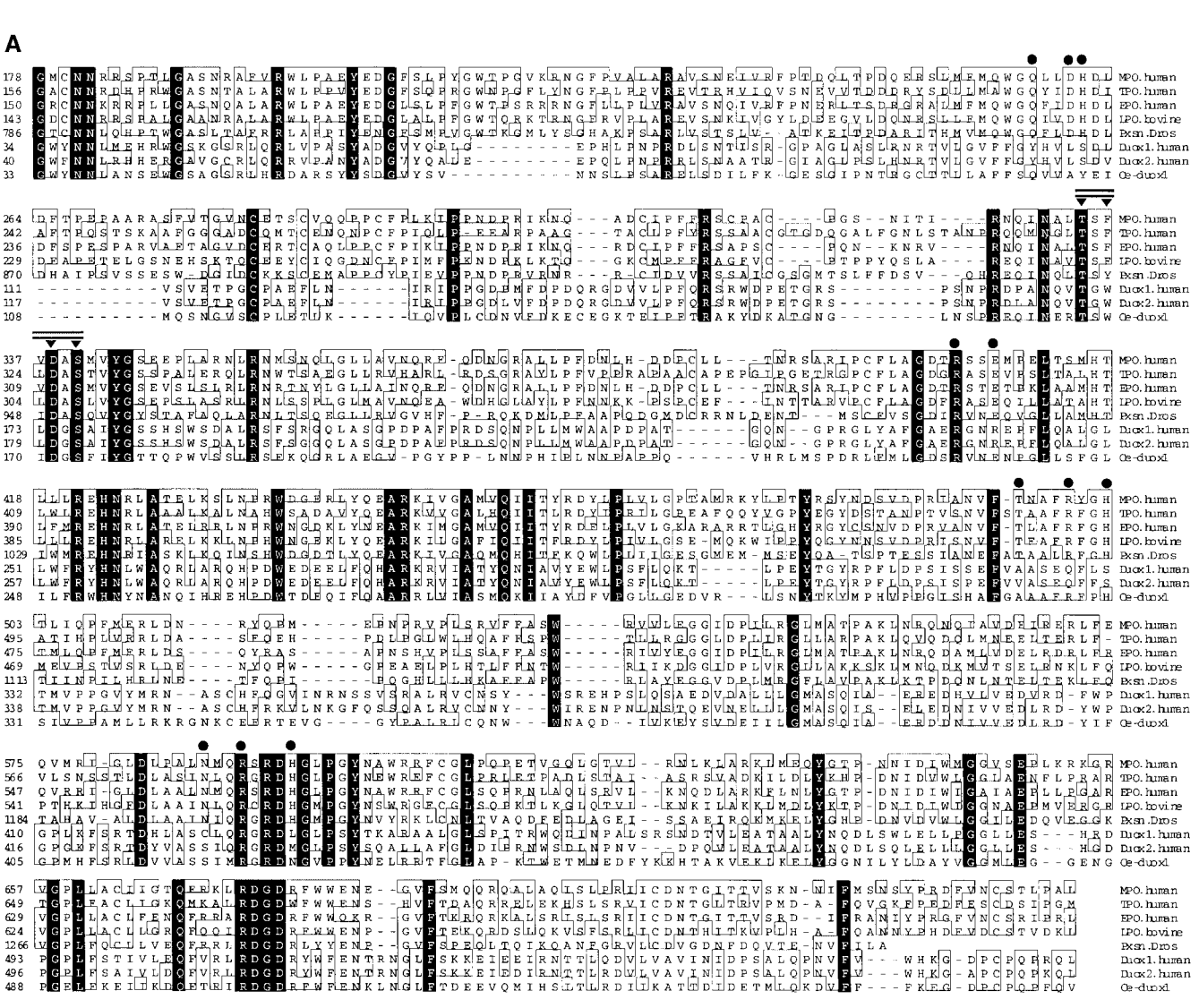

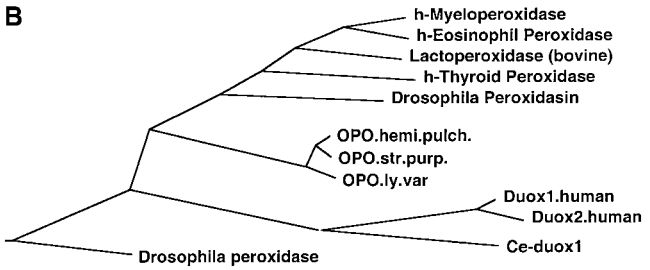

Figure 2. **Comparison of the peroxidase domains of h-Duox, Ce-Duox1, and some known peroxidases**. (A) Sequence alignments. TPO, thyroid peroxidase; EPO, eosinophil peroxidase; LPO, lactoperoxidase, Pxsn.dros, *Drosophila* peroxidasin. Residues which are conserved among all seven proteins are shown with black boxes, whereas those matching a derived consensus sequence are shown in line boxes. Filled circles indicate residues which are proposed to provide contacts with the heme based on the crystal structure of canine MPO (Zeng and Fenna, 1992). The superscripted double bar indicates residues comprising a calcium-binding region, and filled triangles indicate residues which appear in the crystal structure to bind directly to the calcium ion. (B) Phylogenetic relationships. The sequences shown in A and additional sequences are shown. OPO, ovoperoxidase; str.purp, *Strongylocentrotus purpuratus*; ly.var, *Lytechinus variegatus*; hemi.pulch; *Hemicentrotus pulcherrimus*.

a 1,313 amino acid protein. Alignment by homology of the genomic sequences of Ce-Duox1 and Ce-Duox2 identified two new exons 5′ of the first predicted exon of Duox2 that were highly homologous to the second and third exons of Duox1 (predicted cDNA structure available upon request), but an exon of Duox2 homologous to exon1 of Duox1 could not be identified by homology. The predicted amino acid sequences of both Ce-Duox1 and Ce-Duox2 show ~30% identity with h-Duox1 and h-Duox2 (Fig. 1 and Fig. 2 A). Ce-Duox1 also contains the same domains as h-Duox1/2 (see below) and is roughly the same size. However, Ce-Duox2 contains a stop codon, which should eliminate the extreme COOH-terminal portion of the protein, which includes a segment of the pyridine nucleotide-binding site. Thus, whereas Ce-Duox2 should contain intact peroxidase and calmodulin-like domains, it is not predicted to encode a functioning NADPH-oxidase domain (Fig. 1). Except for this COOH-terminal region, Ce-Duox2 is 94% identical to Ce-Duox1 at the amino acid level. Both Ce-Duox1 and Ce-Duox2 are located near the end of chromosome I, separated by only 6 kb and in opposite orientations. The high degree of sequence identity and retention of intron structure (un-

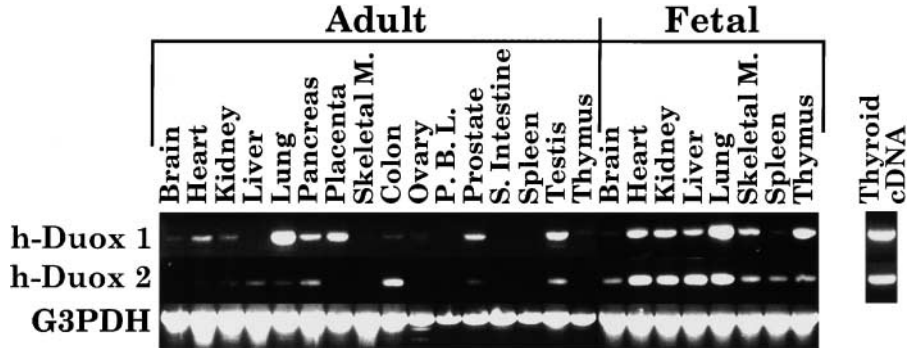

Figure 3. **Tissue expression of mRNA for h-Duox.** mRNA for h-Duox1, h-Duox2, and glyceraldehyde 3-phosphate dehydrogenase were detected by reverse transcriptase PCR as described in Materials and methods.

published data) and the location of both near the end of a chromosome are consistent with a recent gene duplication.

Domain organization and sequence comparisons among gp91*phox*, h-Duox1, Ce-Duox1, and Ce-Duox2

The domain structure and transmembrane regions in gp91*phox*, h-Duox1/2, Ce-Duox1, and Ce-Duox2 are diagrammed in Fig. 1. Duox enzymes are homologous to gp91*phox* in their COOH termini (see http://www.biochem.emory.edu/Lambeth/gp91_homology.pdf for an alignment of these regions). Nox1 (Suh et al., 1999), which is the same size as gp91*phox*, is more closely related to gp91*phox* (54% identical) than is the NADPH-oxidase domain of hDuox1 or h-Duox2 (~26% identical to gp91*phox*). However, h-Duox1 and 2 are more closely related to Ce-Duox1 within the NADPH-oxidase domain (~39% identical). Within the putative flavin adenine dinucleotide (FAD)-binding regions and NADPH-binding regions, homologues share considerably higher homology, ranging from 60 to 90% depending on the region. This includes the canonical dinucleotide-binding helix GXGXXP. In gp91*phox*, Nox1, h-Duox1, and h-Duox2, this sequence is followed by F, which is present in many NADPH-specific flavoproteins, whereas in the *C. elegans* proteins F is conservatively replaced with Y.

Duox proteins have additional regions that are not present in gp91*phox*. A central region contains two EF-hand calcium-binding sequences as indicated in Fig. 1. The canonical residues involved in calcium ligation are well conserved in h-Duox1 and h-Duox2 but are poorly conserved in Ce-Duox1 and Ce-Duox2, suggesting that the function of this region may have evolved away from calcium binding in nematodes.

Surprisingly, the NH_2-terminal third of Duox proteins is homologous to peroxidases including MPO, eosinophil peroxidase, thyroid peroxidase, lactoperoxidase, and sea urchin ovoperoxidases (Fig. 2, A and B). Overall, the identity with peroxidases within the entire region is ~20%, but subregions show considerably higher homology. The Duox enzymes represent a distinct group within the peroxidase family (Fig. 2 B), and phylogenetically this group is marginally more closely related to sea urchin ovoperoxidases. Within the peroxidase homology region, only 2 of the 12 cysteine residues involved in the six intrachain disulfide bonds, which are conserved in the four homologous mammalian peroxidases, are present in Duox proteins (Fig. 2 A). In addition, the asparagine-linked glycosylation sites found in MPO are not present in Ce-Duox1 or Ce-Duox2. A calcium-binding site in MPO (aspartate 263 and residues 335–34; Fig. 2 A, superior double bar) (Zeng and Fenna, 1992) is well conserved in the Duox family proteins, including three of the four candidate calcium liganding residues (Fig. 2 A, ▲).

The extreme NH_2-terminal 21 amino acids of Ce-Duox1 contain a secretory signal peptide sequence (Fig. 1), implying that the NH_2-terminal peroxidase domain is in a compartment that is transmembrane to the cytosol (for example, extracellular or within a secretory vesicle). In addition, hydropathy plots reveal that the proteins contain a highly hydrophobic region corresponding to the NH_2-terminal third of gp91*phox*. This region can be modeled as a cluster of six transmembrane α helices as indicated in Fig. 1. An additional transmembrane helical region is present between the peroxidase homology domain and the calmodulin-like domain.

Tissue distribution of h-Duox mRNA

As shown in Fig. 3, h-Duox1 mRNA was distributed among a variety of adult tissues with highest expression in lung and thyroid but with significant expression also seen in placenta, testis, and prostate, and with detectable expression in pancreas and heart. h-Duox1 mRNA was also widely expressed in fetal tissues where it was abundant in lung. As reported previously (Dupuy et al., 1999), Duox2 ($p138^{Tox}$) is present in thyroid. In addition, we observed significant expression in a variety of fetal tissues and in adult colon with detectable expression in kidney, liver, lung, pancreas, prostate, and testis.

Cellular distribution of Ce-Duox1

The cellular location of Ce-Duox1 was determined by double staining with antibodies to Ce-Duox1 and to the muscle marker myosin A (Fig. 4, A and B). In a longitudinal section, Ce-Duox1 immunostaining was seen in larval animals in a "string-of-pearls" pattern (Fig. 4 A, green) immediately peripheral to muscle (Fig. 4 A, red). Ce-Duox1 (Fig. 4 B, green) was also visualized immediately peripheral to muscle bundles (red) in the cross-sectional plane. Ce-Duox1 staining was considerably weaker in adult animals (unpublished data). The above pattern is consistent with a localization of Ce-Duox1 in hypodermal cells. To verify this localization, double staining was carried out with antibodies to Ce-Duox1 (Fig. 4, C–H, green) and to the hypodermal cell protein MH4 (Fig. 4, C–H, red). Fig. 4, C–E, shows the longitudinal plane, whereas Fig. 4, F and G, shows the cross-sectional plane. Comparison shows that expression of Ce-Duox1 and MH4 occurs in the same cellular pattern, although the staining intensity differed in different regions of the hypodermal cell layer. Merged images are shown in Fig. 4, E and H, and

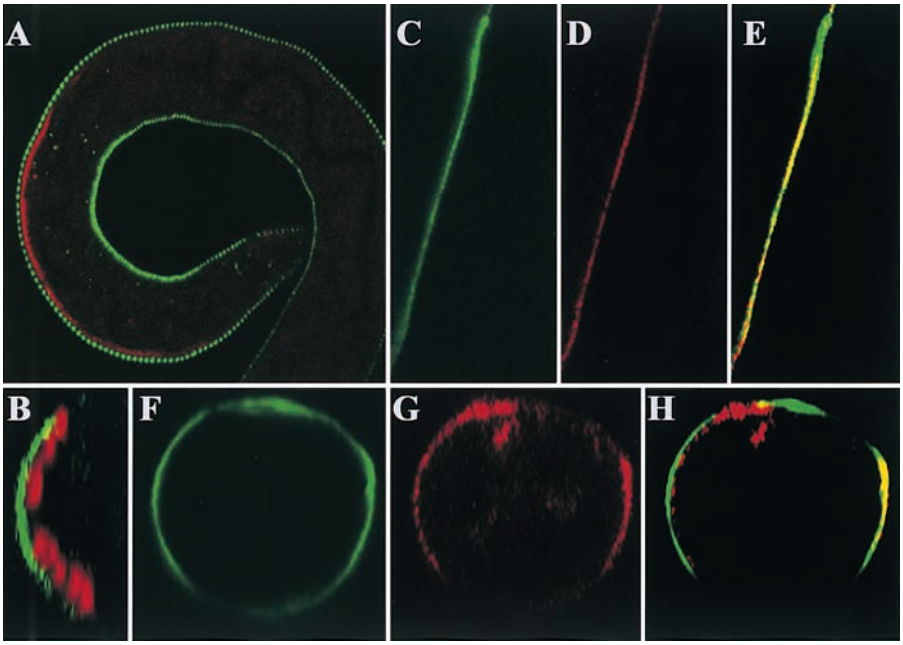

Figure 4. **Cellular expression of Ce-Duox1.** Animals were immunostained with antibodies to Ce-Duox1 (A–C, E, F, and H, green), myosin A (A and B, red), and MH4 (D, E, G, and H, red), and fluorescence was visualized using confocal microscopy. Merged images of Ce-Duox1 and myosin A staining (A and B) show that the Ce-Duox1 is expressed in a layer of cells just outside the muscle bundles. Longitudinal images (C and D) and cross section images (F and G) show the individual staining patters of Ce-Duox1 and the hypodermal cell marker MH4, respectively. Merged images (E and H) show areas of overlapping staining of Ce-Duox1 and MH4 in yellow, confirming the expression of Ce-Duox1 in the hypodermal layer of cells. The use of antibody to Ce-Duox1 that had been preincubated with Ce-Duox1(340–355) peptide eliminated green channel antibody staining (unpublished data). Photos are representative of >100 animals observed.

reveal colocalization in many of the hypodermal cells. Immunostaining with antibody to Ce-Duox1 that had been preincubated with Ce-Duox1(340–355) peptide and antimyosin A antibodies eliminated staining in the green channel (unpublished data), demonstrating antibody specificity.

Phenotypes of *C. elegans* RNAi Ce-Duox animals

To gain insights regarding the biological function of Duox enzymes, we used the reverse genetic tool, RNAi, to "knock out" Duox in *C. elegans* (Fire et al., 1998). This technique involves injection of double-stranded RNA (dsRNA), encoding a segment of Ce-Duox1 or Ce-Duox2 into gonads of *C. elegans* wild-type hermaphrodites. Injected animals were then allowed to lay eggs, the harvested eggs were allowed to develop, and the progeny were observed for phenotypes. This procedure specifically diminishes or eliminates the expression of the gene of interest. dsRNA corresponding to three distinct regions of Ce-Duox1 and Duox2 were used in separate experiments. The first two correspond to regions of identity between Ce-Duox1 and Ce-Duox2 and are predicted to block the expression of both forms of Duox. The third dsRNA corresponds to the extreme COOH terminus of Ce-Duox1, which does not have a counterpart in Ce-Duox2, and therefore blocks only the expression of Ce-Duox1. All three dsRNA forms resulted in the same range of phenotypes. In replicate experiments, the percentage of animals exhibiting any given phenotype was somewhat variable, probably due to differences in amount of RNAi or site of injection. However, in a typical experiment >90% of the animals were affected by one or more phenotypes. In a typical experiment, phenotypes included the presence of large superficial blisters (Fig. 5 B, ~50% of animals) and short or "dumpy" animals (Fig. 5 C, ~35% of animals) and animals with retained eggs or larvae (unpublished data). In addition, whereas wild-type animals showed a dark appearance, >80% of RNAi animals were translucent (compare wild-type, Fig. 5, A and D, animal on right with affected animals in D, animal on left, and B and C). Around half of RNAi animals showed an inability to move on plates in a normal serpentine manner: affected animals were either completely paralyzed or moved only the anterior region, clearing a localized swath of *Escherichia coli* in the vicinity of the head (Fig. 5, B and C).

Similar phenotypes in *C. elegans* have been described previously and are associated with mutations in the collagen biosynthetic pathway (Levy et al., 1993; Grupta et al., 1997; Johnstone, 2000). Several genes that encode cuticle collagens when mutated result in Bli ("blister"), Dpy ("dumpy," short fat worm), Rol ("roller," helical motion instead of a flat, sinusoidal motion), or Sqt ("squat," generally rollers as larvae and dumpy as adults) phenotypes. The genetics of this process are complex, since for some genes different mutations in the same gene give rise to different phenotypes, and sometimes the phenotypes are combined (for example, "dumpy roller"). In nematodes, collagen along with several other proteins provide the major components of cuticle, an extracellular matrix which acts as an exoskeleton. In a global analysis of expression of all *C. elegans* genes using oligonucleotide arrays (Hill et al., 2000), Ce-Duox1 was expressed at low levels (consistent with its exclusive expression in hypodermal cells) in a stage-specific manner. Expression occurred in a cyclic pattern, peaking during the embryonic stage and at 36 h, corresponding to the peak expression of other genes (Johnstone, 2000) related to collagen/cuticle biosynthesis (*col-14*, *dpy-2,-7,-10*, and *sqt-3*). A second set of collagen/cuticle-related genes (*bli-1*,*-2*, *col-2, -6,-17,-35,-36,-37,-41*, *dyp-13*, *sqt-1*, and *rol-6,-8*) also show peak expression at 36 h. No significant expression of Ce-Duox2 was seen at any stage. Thus, these data are consistent with a function of Ce-Duox1 in cuticle biogenesis.

The similarity in phenotypes among animals defective in collagen and cuticle biosynthesis compared with the RNAi Duox animals suggested that Duox participates in cuticle biogenesis. To confirm this hypothesis, EM was carried out on wild-type and RNAi animals. As shown in Fig. 6, cuticle of RNAi Duox animals was grossly abnormal. In normal animals (Fig. 6 A), three cuticle layers are

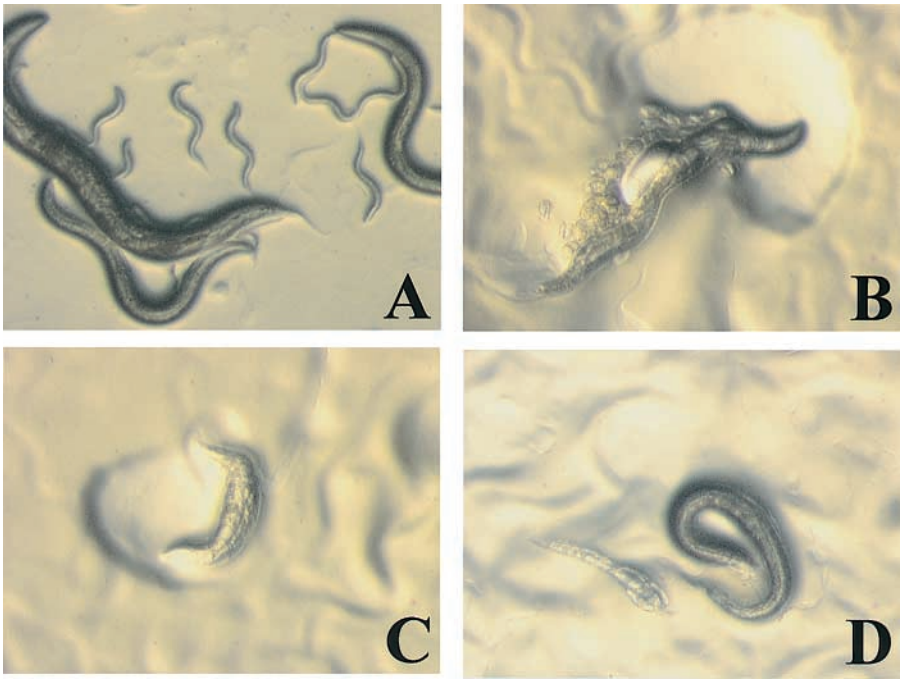

Figure 5. **Loss of function phenotypes of Ce-Duox1 resulting from RNAi**. (A) Wild-type animals showing normal morphology and sigmoidal shape. (B) Mutant animal showing a large blister and defect in movement evidenced by local expulsion of eggs and local clearing of bacteria near the anterior of the worm. (C) Mutant worm showing a "dumpy"-like phenotype and local clearing of the bacterial lawn. (D) Mutant worm on left demonstrating translucent appearance compared with wild-type worm on right. Duox1 dsRNA was injected into N2 hermaphrodites in six independent experiments. In each, although the resulting phenotypes showed a range of severities the phenotypes were identical.

seen clearly: the cortical (outer), median, and basal (inner) layer as described previously (Cox et al., 1981). The median layer is composed of struts (Fig. 6 A, arrows) connecting the cortical and basal layers with a fluid-filled space between these layers. The RNAi animals (Fig. 6, B and C) frequently showed separation between the cortical and the basal layers with marked expansion of the fluid cavity and broken and distended struts that are still visible on these layers (Fig. 6 B, arrows). These separations occurred mainly over bundles of muscle fiber (Fig. 6, B and C) and are likely to account for the formation of the blisters seen by light microscopy. Thus, the cuticle structure was severely affected in RNAi Duox animals.

Absence of tyrosine cross-linking in RNAi nematodes

Cross-linking of collagen and other cuticle proteins in nematodes occurs through di- and trityrosine linkages, which bridge and stabilize the proteinaceous structure (Fetterer and Rhoads, 1990; Fetterer et al., 1993). Because peroxidases such as sea urchin ovoperoxidase and human MPO carry out this reaction (LaBella et al., 1968; Malanik and Ledvina, 1979; Deits et al., 1984), we hypothesized that the function

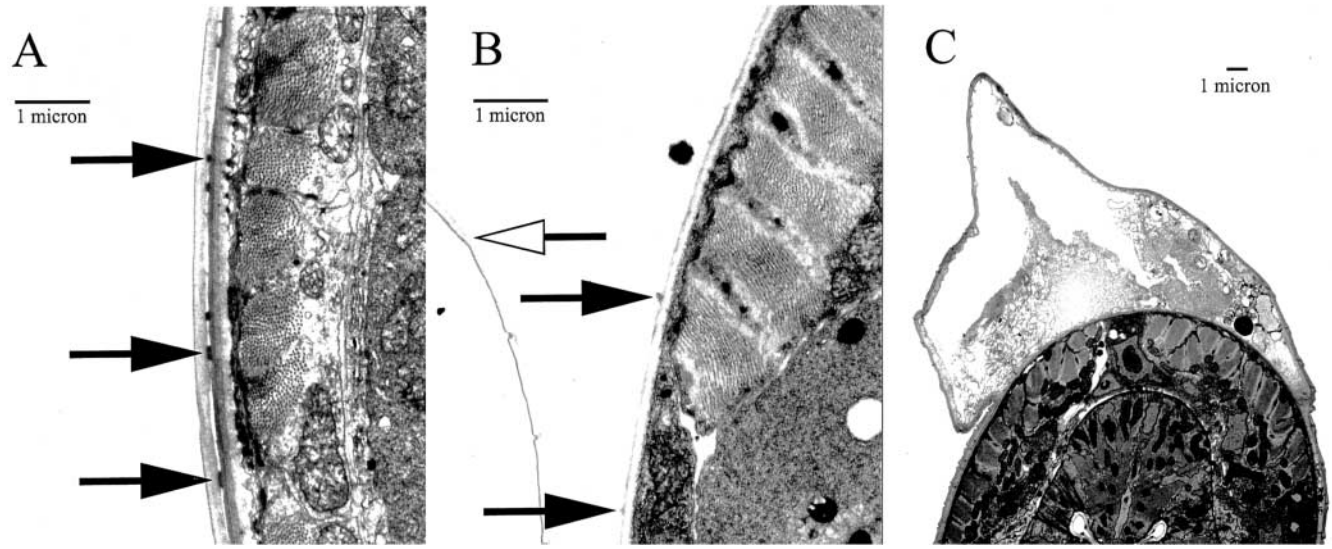

Figure 6. **EM of Ce-Duox RNAi animals.** (A) Cross-sectional view of wild-type animals showing normal cuticle structure. Arrows indicate the location of struts. (B) Cross-sectional view of an RNAi animal showing separation of the cuticle into two layers. Solid arrows indicate broken struts attached to the basal layer, and the open arrow indicates the cortical layer that has detached from the basal layer. (C) Cross-sectional view of a RNAi animal showing the full view of a blister. The animals shown are representative of 10 in each group. Magnification was 8,155× (C) and 12,575× (A and B).

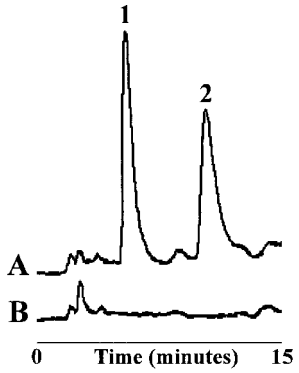

Figure 7. **Absence of di- and trityrosine linkages resulting from RNAi**. Total protein from wild-type (A) and RNAi (B) animals was extracted, hydrolyzed, and analyzed by HPLC monitoring fluorescence. Peak 1 was identified as dityrosine, and peak 2 was identified as trityrosine as described. The experiment is representative of three.

of Ce-Duox1 (and possibly Ce-Duox2) is to generate tyrosine cross-links and that the defective cuticle in the Ce-Duox RNAi animals is due to an inability to form tyrosine cross-links. A role for an unknown peroxidase in tyrosine cross-linking in *Ascaris* was suggested previously based on studies in which tyrosine cross-linking activity was inhibited using the peroxidase inhibitors 4-amino-2,3,4 aminotriazole, phenylhydrazine, and *N*-acetyl tyrosine (Fetterer et al., 1993). We therefore examined the wild-type and Ce-Duox1/2 RNAi knockout animals for di- and trityrosine linkages. An HPLC profile of an acid hydrolysate of the wild-type *C. elegans* is shown in Fig. 7, trace A. The first large peak was identified as dityrosine based on comparison with authentic standard and mass spectral analysis, and the second peak is identified as trityrosine based on its migration on HPLC relative to dityrosine and mass spectral analysis. Based on peak areas and assuming equivalent ionization, dityrosine and tyrosine were present in a ratio of 1:200 in adult wild-type animals. In addition, the fluorescence excitation/emission maxima were determined at alkaline and acidic pH and were in good agreement with previously reported values (Jacob et al., 1996). Mass spectral analysis of purified *C. elegans* cuticle and noncuticular material determined that >99.99% of dityrosine and trityrosine are located in cuticle material, since dityrosine was undetectable in the noncuticle fraction (unpublished data). Dityrosine and trityrosine peaks were absent in hydrolysates of Ce-Duox RNAi nematodes (Fig. 7, trace B). Thus, interference with the expression of Ce-Duox1 eliminates formation of di- and trityrosine linkages.

Biochemical activities of the expressed peroxidase domains of Ce-Duox1 and h-Duox1

The peroxidase domains of Ce-Duox (residues 1–590) and h-Duox1 (residues 1–593) were expressed in *E. coli* as described in Materials and methods. A lysate from these cells was analyzed for peroxidase activity, and the results are summarized in Fig. 8 A. As shown, the lysates from *E. coli* expressing both the human and the *C. elegans* peroxidase homology domains from Duox demonstrated peroxidase activity towards 3,3′,5,5′-tetramethylbenzidine (TMB), a well-

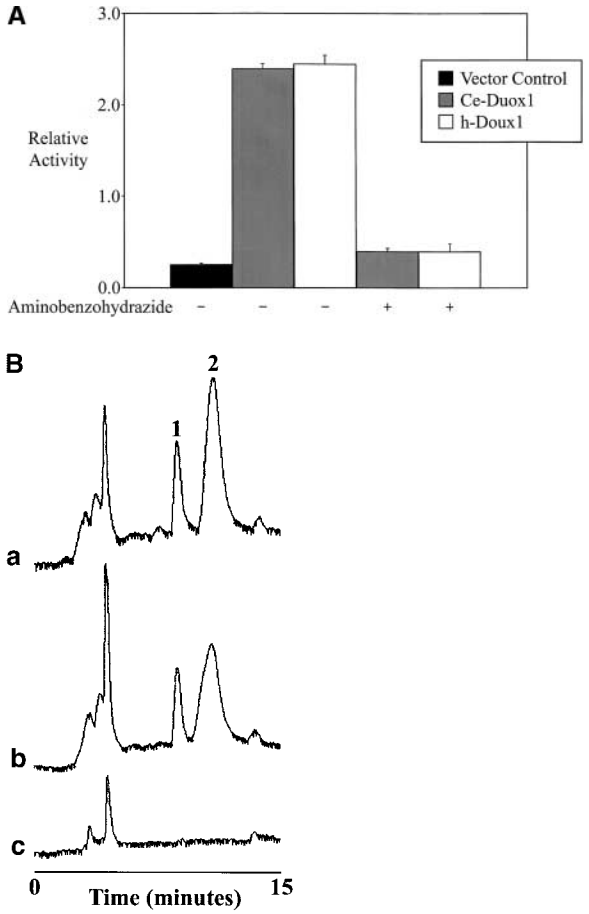

Figure 8. **Biochemical activities of Duox peroxidase domains**. Peroxidase domains from h-Duox1 and Ce-Duox1 were expressed in *E. coli* as described in Materials and methods. (A) Lysates (100 μg protein) from vector control *E. coli* or *E. coli* expressing Ce-Duox or h-Duox were added to an assay mixture containing tetramethylbenzidine and hydrogen peroxide, the mixture was incubated at 25°C for 2 min, and the optical density was read at 655 nm. Some incubations contained 30 μM aminobenzohydrazide. (B) Lysates (100 μg protein) from *E. coli* from vector control cells (c) or cells expressing Ce-Duox1 (a) or h-Duox1 (b) were incubated at 25°C for 60 min with tyrosine ethyl ester. The reaction was quenched, and the ester was hydrolyzed as described in Materials and methods. The product was analyzed by HPLC, monitoring fluorescence, and the results are representative of three experiments. Peak 1 is dityrosine, and peak 2 is trityrosine as in Fig. 7.

characterized peroxidase substrate. The activity was inhibited by the peroxidase inhibitor aminobenzohydrazide. Lysates from *E. coli* expressing the peroxidase domains of h-Duox and Ce-Duox but not those from vector control cells also catalyzed the cross-linking of tyrosine ethyl ester (Fig. 8 B). Two major fluorescent products were seen; peak 1 was identified by cochromatography with authentic material and mass spectral analysis as dityrosine, whereas peak 2 was identified as trityrosine by mass spectral analysis as above.

Discussion

The topology model shown in Fig. 9 is proposed for Duox based on its primary structure and on analogy with known features of gp91*phox*. In activated phagocytes, gp91*phox* is inte-

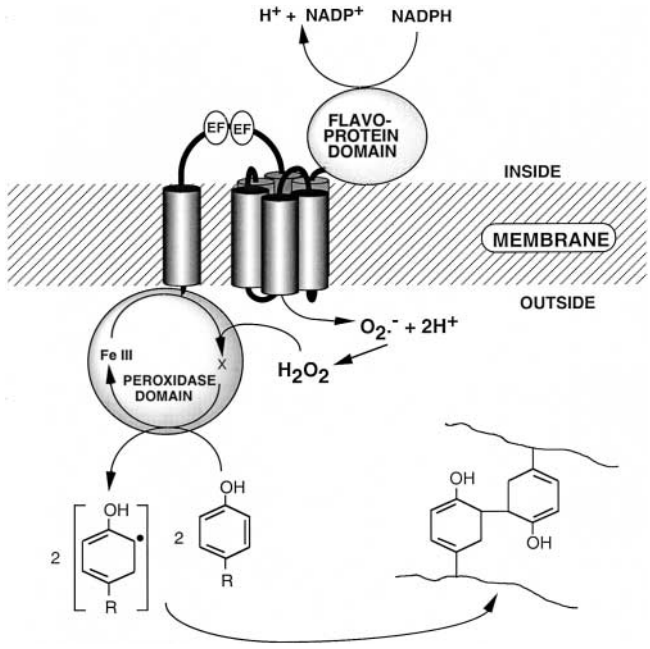

Figure 9. **Proposed topology model for Duox.** See text for details.

grally associated with the plasma membrane. The COOH-terminal half of gp91*phox* is homologous to known FAD proteins (Rotrosen et al., 1992; Segal et al., 1992; Sumimoto et al., 1992) and contains a predicted NADPH-binding site. This region is thus likely to fold into a discrete intracellular flavoprotein domain. Gp91*phox* also contains an NH_2-terminal hydrophobic domain, comprising nearly half of the molecule. The corresponding region in Duox is predicted to cross the membrane six times (Fig. 1 A), placing both the NH_2 terminus and the COOH terminus (attached to the flavoprotein domain) on the cytosolic side. Several features of the model have been verified for gp91*phox*. For example, the model places known glycosylation sites on the cell exterior (Wallach and Segal, 1997) and a binding loop for the cytosolic regulatory protein p47*phox* (Biberstine-Kinkade et al., 1999) on the cytosolic side.

The gp91*phox* homology domains in h-Duox1/2 and Ce-Duox1/2 show the same hydropathy profile and predicted transmembrane α helices as gp91*phox* (Fig. 1, hashed bars within the gp91*phox* homology region). We therefore assume that the gp91*phox* transmembrane model will also apply to the COOH-terminal portion of the Duox proteins. Such a model predicts that the domain containing the EF-hands is on the interior of the cell. The presence of a secretion export signal peptide sequence at the extreme NH_2 terminus (Fig. 1 A) and the presence of an additional predicted transmembrane hydrophobic sequence intervening between the EF-hand domain and the peroxidase homology domain predicts that the peroxidase domain will reside on the exterior of the cell (Fig. 9). Although features of this model will need to be tested directly, this structure is attractive as it is consistent with the genetic and biochemical data, implicating Ce-Duox1 in the generation of extracellular tyrosine cross-links in cuticle proteins.

The phagocyte NADPH-oxidase serves as a model for the function of the gp91*phox* homology domain of Duox. The gp91*phox* component of the phagocyte oxidase generates reactive oxygen outside of the cell or in the phagosome (which is topologically extracellular). NADPH reduces the FAD within the flavoprotein domain, and the FAD then passes electrons through the two heme groups located within the transmembrane NH_2 terminus of gp91*phox*, reducing oxygen to form superoxide outside of the cell with secondary production of hydrogen peroxide by dismutation. Such a function has been demonstrated for $p138^{Tox}$ (Duox2), which was purified as the hydrogen peroxide–generating NADPH oxidase from thyroid (Dupuy et al., 1999). These authors proposed that $p138^{Tox}$ functions to provide H_2O_2 to thyroid peroxidase, which is known to iodinate the thyroid hormone precursor. A recent study (De Deken et al., 2000) identified a peroxidase homology domain in Duox1 and Duox2 (ThOX1 and ThOX2), but the authors suggested that this domain was inactive based on an absence of putative catalytically important residues.

Oxidative reactions are generally thought to be deleterious to the cell, but the results of the current study suggest that protein oxidation by peroxidases plays a critical role in normal physiology. Insights into the function of the Duox peroxidase domain come from the phagocyte system in which cell activation is accompanied by both activation of the phagocyte NADPH-oxidase and secretion of MPO. Hydrogen peroxide generated indirectly by the phagocyte NADPH-oxidase combines with chloride in an oxidation catalyzed by MPO to form hypochlorous acid, a species which functions in bactericidal reactions. In the case of Duox enzymes, both the NADPH-oxidase moiety and the peroxidase moiety are integrated into a single molecule. The hydrogen peroxide generated by the gp91*phox*-homology domain in Duox should then serve as a substrate for the peroxidase domain. For Ce-Duox1, the cosubstrate is protein tyrosine residues, which are converted to di- and trityrosine presumably via a reaction involving the tyrosyl radical based on mechanisms established for other well-studied peroxidases; tyrosyl radical recombination would generate di- and trityrosine, resulting in protein cross-linking to stabilize the nematode cuticle. Peroxidases including human MPO (Heinecke et al., 1993) and the sea urchin ovoperoxidase (Deits et al., 1984) catalyze this tyrosine cross-linking, albeit in the former case somewhat inefficiently. Thus, the proposed topological structure of Duox is well suited to support transmembrane peroxidative reaction using intracellular reducing equivalents from NADPH.

Precedent for the involvement of a peroxidase in extracellular matrix structure comes from the fertilization reaction in sea urchin oocytes. Fertilization results in activation of tyrosine cross-linking of extracellular proteins in the oocyte, forming a protective fertilization envelope (Deits et al. 1984). This reaction is catalyzed by ovoperoxidase, a peroxidase secreted by the oocyte. In this system, the hydrogen peroxide is generated by an unknown NADPH-oxidase. Thus, in the case of the sea urchin oocyte individual proteins carry out the peroxide generation and the peroxidative functions respectively. Yeast spore coats also contain dityrosine cross-links that are formed by a heme protein (Briza et al. 1996).

The closest known structural homologues of h-Duox1/2 are Ce-Duox1 and Ce-Duox2. Both h-Duox1/2 and Ce-Duox1 show the same domain structure, including the gp91*phox* homology domain, the EF-hand domain, and the

peroxidase domain. In the case of h-Duox1/2, the critical calcium-binding residues in the EF-hand domain are well conserved, suggesting a role for calcium in the regulation of the enzyme activity. This has been proposed to account for the calcium dependence for the NADPH-oxidase activity of $p138^{Tox}$ (Duox2), (Dupuy et al., 1999). In contrast, the calcium-binding ligands in the EF-hand regions in Ce-Duox1/2 are poorly conserved, suggesting that calcium may not be involved at this site. Calcium-binding regions within the peroxidase domain are well conserved in both Ce-Duox1/2 and h-Duox, suggesting a distinct role for calcium as has been noted for other peroxidases.

The similarity between the peroxidase domain of Ce-Duox1 and h-Duox1/2 raises the possibility that their function will be similar. The peroxidase domains of h-Duox1/2 and Ce-Duox1 are 37% identical to one another, whereas the peroxidase domains of Duox proteins are only 19–20% identical with known mammalian peroxidases. Thus, among known peroxidases or peroxidase domains the h-Duox is most similar to Ce-Duox1, and this may imply similar catalytic specificities. Supporting this idea, biochemical data show that the recombinant-expressed peroxidase domains from human and *C. elegans* Duox are both capable of generating di- and trityrosine cross-links. This conservation of domain structure, sequence, and biochemical activity is suggestive of a similar function for Ce-Duox1 and h-Duox1/2. In addition, our data showing that Duox1 and Duox2 expression is not restricted to thyroid suggests that their function is not limited to a thyroid-specific function. In thyroid, the peroxidase domains of h-Duox1 and h-Duox2 may participate in iodination of thyroglobulin, the precursor of thyroxine. If this is the case, then the function is redundant to that of the well-characterized thyroid peroxidase (Taurog, 1999). However, because other tissues in which Duox1/2 are expressed lack iodine uptake systems such a function in these tissues seems unlikely. In addition to iodination, mammalian Duox might also function in forming the ether bridge of thyroid hormone, a reaction that is analogous to pulcherosine synthesis.

Is mammalian Duox involved in generation of tyrosine cross-links? Dityrosine cross-links stabilize several types of extracellular matrices including not only the cuticle of nematodes (above), but also insect elastomer resilin (Anderson, 1963), insect cuticle (Locke, 1969; Hall, 1978; Klebanoff et al., 1979; Deits et al., 1984), the chorion envelope of *Drosophila* eggs (Georgi and Deri, 1976; Mindrinos et al., 1980), and the yeast acrospore wall (Briza et al., 1996). The occurrence of dityrosine and a possible role in extracellular matrix in mammalian system is less well studied. In mammals, dityrosine is a marker of inflammation as occurs in low density lipoprotein isolated from atherosclerotic plaques (Leeuwenburgh et al., 1997). Dityrosine is proposed to be formed during inflammation through the action of MPO secreted by inflammatory cells (Zaitsu et al., 1981) or in the mouth by salivary lactoperoxidase (Tenovuo and Paunio, 1979), but Duox-dependent mechanisms are not ruled out. A major constituent of extracellular matrix and basement membrane is collagen, and mammalian collagen has been reported previously to contain very low concentrations of dityrosine linkages (~1 in 100,000 tyrosines) (Keeley et al., 1969; Waykole and Heidemann, 1976), in addition to the predominant cross-links involving lysines and histidines. However, such cross-linking may be nonspecifically associated with aging or artifactually induced during sample preparation. Dityrosine linkages have been isolated from other structural proteins and hard tissues such as elastin (LaBella et al., 1967), fibrin and keratin (Raven et al., 1971), and cataractous human lens protein (Garcia-Castineiras et al., 1978). In elastin, although the predominant cross-link involves lysine it has been speculated that the tyrosine cross-links may be critical at early stages of elastin biogenesis and that this is followed later by extensive cross-linking at lysines (LaBella et al., 1967). Low concentrations of tyrosine cross-links might help order and align elastin and/or collagen fibrils, aligning further high abundance cross-linking at lysines. Such a role for human Duox is attractive and is consistent with its expression in lung, which possesses a high content of elastin. To our knowledge, dityrosine linkages in mammalian basement membrane or extracellular matrix other than collagen and elastin have not been described, perhaps owing to a lack of sufficient quantities of material for analysis. In addition, another peroxidase-catalyzed cross-link is formed from the deamination of protein lysyl ϵ-amino groups to form lysyl aldehydes, which then react with amino acid residues of adjacent molecules (Stahmann et al., 1977; Clark et al., 1986; Hazen et al., 1997). Thus, it is also possible that h-Duox generates this type of extracellular matrix cross-link. Its transmembrane nature and results from RNAi studies in *C. elegans* support the hypothesis that this enzyme participates in the formation or modification of extracellular protein matrix.

Materials and methods

Cloning of the cDNA for human Duox1

A BLAST search using as a query the NH_2-terminal region of a partial clone of Duox2 (see below) identified a 357 base-sequenced portion of an expressed sequence tag (EST, nr80d12.s1; sequence data available from GenBank/EMBL/DDBJ under accession no. AA641653) from an invasive human prostate tumor. The bacterial strain containing the EST sequence in the pBluescript SK-vector was purchased from American Type Culture Collection. The DNA sequenced using T7 and T3 vector primers and sequence-specific primers. The EST insert encoded an ORF of 673 amino acids but lacked both candidate start and stop codons. Northern blot analysis indicated the mRNA was ~5.5 kb. 5′ rapid amplification of cDNA ends (RACE) and 3′ RACE were carried out using human adult lung mRNA (CLONTECH) as template. 5′ RACE was carried out with a 5′ RACE kit (version 2.0; GIBCO BRL) using sequence-specific primers: 5′ RACE, 5′-GCAGTGCATCCACATCTTCAGCAC-3′ and 5′-GAGAGCTCTGGAGACACTTGAGTTC-3′ (for nested PCR). 3′ RACE was carried out with sequence-specific primers: 5′-CATGTTCTCTCTGGCTGACAAG-3′ and 5′-CACAATAGCGAGCTCCGCTTCACGC-3′ (for nested PCR). 5′ RACE yielded 1.1 kb, and 3′ RACE yielded 2.4 kb of new DNA sequence. These procedures generated a sequence, which predicted an ORF of 4,563 base pairs, which encodes a predicted 180-kD protein comprised of 1,521 amino acids.

Cloning of the cDNA for human Duox2

A 535 base portion of an EST (zc92h03.rl; sequence data available from GenBank/EMBL/DDBJ under accession no. W52750) from human pancreatic islet was identified using the amino acid sequence of human gp91*phox* as a query in a BLAST search. The bacterial strain no. 595758 containing the EST sequence zc92h03.rl in the pBluescript SK-vector was purchased from American Type Culture Collection. The DNA was sequenced using primers to T7 and T3 vector promoters and sequence-specific internal primers. The EST encoded a 440 amino acid partial cDNA exhibiting 24.4% identity to gp91*phox*, including a stop codon corresponding to the COOH terminus of gp91*phox*. 5′ and 3′ RACE were carried out using human adult pancreas mRNA (CLONTECH) with the 5′ RACE kit for Rapid

Amplification of cDNA ends version 2.0 (GIBCO BRL). PCR was done with specific primers: 5′ RACE: primer 1, 5′-GAAGTGGTGGGAGGCGAAGACATA-3′; primer 2, 5′-CCTGTCATACCTGGGACGGTCTGG-3′; primer 3, 5′-GAGCACAGTGAGATGCCTGTTCAG-3′; primer 4, 5′-GGAAGGCAGCAGAGAGCAATGATG-3′; primer 5, 5′-AGGTGGGATGCGGATGTTGAG-3′ (for nested PCR); 3′ RACE primer 6, 5′-ACATCTGCGAGCGGCACTTCCAGA-3′; primer 7, 5′-AGCTCGTCAACAGGCAGGACCGAGC-3′; primer 8, 5′-TCTCCATCAGAATCCACCTTAGGC-3′ (for nested PCR). To complete the sequence, 5′ RACE was carried out using human thyroid marathon-ready cDNA (CLONTECH) with primer 3 and adapter primer AP1 and primer 5 and adapter primer AP2. These procedures resulted in an additional 3.7-kb 5′ region and a 1.5-kb 3′ region.

Identification of genes for Ce-Duox1 and Ce-Duox2

A BLAST search using the cDNA sequence of human gp91*phox* identified two putative homologues (sequence data available from GenBank/EMBL/DDBJ under accession nos. AF043697 and AF003130) in the genomic sequence of *C. elegans*, both near the end of chromosome I and separated by ~6 Kb.

Cloning of the cDNA for Ce-Duox1

Based on the gene sequence, PCR primers were designed to amplify two overlapping portions of the Ce-Duox1 gene: one extending from the 5′ end and one extending from the 3′ end. Primers were 5′-ATTCGTCGACAAATGCGCTCAAAACATGTGCTGT-3′ and 5′-AACTTTGTGGATCAAAGTTAGCG-3′ for the 5′ region, and 5′-TTGGATTAGCATTTTGCTATGGAA-3′ and 5′-GAGCGGCCGCGAACGTTTCAAAGCGATGTGCA-3′ for the 3′ region. PCR was carried out using a random primed *C. elegans* cDNA library in λACT (obtained from R. Barstead, Oklahoma Medical Research Foundation, Oklahoma City, OK) under the following conditions: denaturation at 95°C for 30 s, annealing at 59°C for 30 s, and extension at 72°C for 1 min. The 5′ piece and the 3′ piece were digested with Dra III and ligated to produce the full-length Ce-Duox1 cDNA. The full-length Ce-Duox1 cDNA was inserted into the pBluescript SK-vector and was sequenced using T7 and T3 vector primers and sequence-specific primers.

Analysis of primary structure

Export signal sequences were predicted according to Nielsen et al. (1997). Transmembrane α helices were predicted according to Sonnhammer et al. (1998). Both methods are available on the internet at the Center for Biological Sequence Analysis (http://www.cbs.dtu.dk/services). Multiple sequence alignments phylogenetic analysis were carried out using the clustal method using Megalign software (DNASTAR).

PCR detection of mRNA for human Duox

Based on the cloned h-Duox1 and hDuox2 cDNA sequence, we designed specific primers (Duox1: 5′-GCAGGACATCAACCCTGCACTCTC-3′ and 5′-CTGCCATCTACCACACGGATCTGC-3′; Duox2: 5′-GCCCTCAACCTAAGCAGCTCACAACTG-3′ and 5′-GAGCACAGTGAGATGCCTGTTCAG-3′), which were used to determine the tissue expression patterns of Duox1 and Duox2 using human multiple tissue PCR panels and human thyroid gland marathon-ready cDNA (CLONTECH). PCR conditions were as follows: 95°C for 30 s, 65°C for 20 s, and 72°C for 30 s, for a total of 35 cycles.

RNAi in *C. elegans*

The procedure was taken from Fire et al. (1998). RNA was transcribed from either pBluescript.Duox2, pBluescript.E17Duox1, or pBluescript.E18 + 19Duox1. For pBluescript.Duox2, exon 10 of Ce-Duox2 was amplified by PCR from genomic DNA using the forward primer 5′-GCTAGAGCTCTTCAGTTTGCTATGGAATTGGC-3′ and reverse primer 5′-CATAAAGGATGAGGAGAATTCTGTG-3′. The 457-bp fragment generated was digested with SstI and EcoRI and subcloned into pBluescript. For pBluescript.E17Duox1, exon 17 of Duox1 was amplified by PCR from genomic DNA using the forward primer 5′-GCTAGAGCTCGGCTACTACTACGTTGTTGGACC-3′ and the reverse primer 5′-GACTGAAGGACTTGTGGAACGTCTGAGTGAC-3′. The 659-bp fragment generated was digested with SstI and EcoRI and subcloned into pBluescript. For pBluescript.E18 + 19Duox1, exons 18 and 19 of Ce-Duox1 were amplified by PCR from a randomly primed *C. elegans* cDNA library (obtained from R. Barstead, Oklahoma Medical Research Foundation) using the forward primer 5′-GCTAGAGCTCACATTTGCGAGAAGCACTTCCG-3′ and the reverse primer 5′-GTGTGAATTCAGCGATGTGCAAATGAAGGAGC-3′. The 266-bp fragment generated was digested with SstI and EcoRI and subcloned into pBluescript. Plasmids were linearized with either Sst1 or EcoR1, and transcription was carried out using T3 and T7 RNA polymerase (Promega) in separate reactions. Sense and antisense single-stranded RNAs were combined in equal concentrations and incubated for 10 min at 68°C followed by a 30 min incubation at 37°C to form dsRNA. dsRNAs were injected into the gonads of N2 hermaphrodite *C. elegans*. Injected animals were allowed to recover and lay eggs for ~20 h after injection, transferred to individual plates, and allowed to lay eggs for a second 24-h period. The F1 progeny resulting from this second period of egg laying were evaluated. Phenotypes were observed in >90% of F1 animals.

Antibody production and purification

A 16 amino acid peptide corresponding to residues 340–355 of Ce-Duox1 was synthesized by the Emory Microchemical Facility and coupled using gluteraldehyde to keyhole limpet hemocyanin. Rabbit antibody was prepared against keyhole limpet hemocyanin–conjugated peptide by Lampire Biological Laboratories using standard protocols. Peptide (30 mg) was coupled to 1 ml of Affi-Gel 10 (Bio-Rad Laboratories) for antibody immunopurification; 2 ml of serum was dialyzed against PBS and was loaded onto the Affi-Gel column preequilibrated with PBS. The column was washed with 10 ml PBS containing 1 M NaCl. 0.5 ml-factions of antibody were eluted with 0.1 M glycine-HCl (pH 2.4) and were immediately neutralized with Tris, pH 9. Fractions containing the highest concentration of protein were used in immunofluorescence experiments.

Western blot

Nematodes were washed with M9 buffer, suspended in 0.5 ml sonication buffer (10 mM Tris HCl, pH 7.4, 1 mM EDTA, 1 mM phenylmethanesulfonyl fluoride) and sonicated four times for 20 s. Protein was determined with the Bradford assay using BSA as a standard. 10 μg of whole animal extract was loaded onto a 10% SDS-page gel, which was then transferred to Immobilon-P membrane (Millipore). The blot was blocked for 1 h in a solution of 5% nonfat powdered milk and 0.05% Tween in PBS. The antibody to Ce-Duox1 was added in a 1 to 2,000 dilution, incubated overnight, and the membrane was washed three times for 15 min with blocking solution. The blot was then developed using the SuperSignal chemiluminescent kit from Pierce Chemical Co. A Western blot of *C. elegans* protein extract showed a single band with a molecular weight of ~180,000 (unpublished data).

Indirect immunofluorescence

Immunofluorescence staining of *C. elegans* was carried out as in Benian et al. (1996). Goat anti–mouse rhodamine-conjugated antibody and goat anti–rabbit FITC-conjugated antibody were used as secondary antibodies for the detection of Ce-Duox1 antibody, myosin A antibody, and MH4 antibody. Mouse antibody to myosin A was a gift from D. Miller (Vanderbilt University, Nashville, TN) (Miller et al., 1983). The MH4 monoclonal antibody developed by G.R. Francis and R.H. Waterston (Washington University, St. Louis, MO) (Francis and Waterston, 1991) was obtained from the Developmental Studies Hybridoma Bank developed under the auspices of the National Institute of Child Health and Human Development and maintained by The University of Iowa, Department of Biological Sciences. To determine nonspecific binding of the Ce-Duox1 antibody, a 10-fold molar excess of Ce-Duox1(340–355) peptide was added to neutralize the antibody. Microscopy was carried out using ZEISS 510 laser scanning confocal microscope.

Preparation of dityrosine standard

Dityrosine standard was synthesized and purified as in Abdelrahim et al. (1997) with minor modifications. Reaction products were dissolved in acidified methanol, filtered, and directly applied to the CP-11 cellulose phosphate, eliminating the rotary evaporation step. Samples with absorption properties characteristic of dityrosine were pooled and freeze dried. For mass spectrometry, the 1 ml of dityrosine standard (0.77 mg/ml) was added to 1 ml of methanol–water (1:1) in 0.1% acetic acid.

Analysis of dityrosine and trityrosine

Nematodes were washed with M9 buffer, suspended in 0.5 ml sonication buffer (10 mM Tris HCl, pH 7.4, 1 mM EDTA, 1 mM phenylmethanesulfonyl fluoride), and sonicated four times for 20 s. Protein was determined with the Bradford assay using BSA as a standard. Whole worm extracts were lyophilized and resuspended in 6 N HCl. Samples were hydrolyzed for 24 h at 110°C under vacuum, dried under vacuum, and resuspended in the mobile phase for analysis by HPLC on a C18 column (0.46 × 26 cm; Fisher Scientific) using a Dionex AGP-1 HPLC instrument. The mobile phase consisted of 0.1 M KH_2PO_4 adjusted to pH 3.8 with 0.1 M phosphoric acid at a flow rate of 1 ml/min. The column eluent was monitored by fluorescence with an excitation 305–395-nm bandpass filter and an emission filter at 450 nm with a bandpass of 40 nm. To verify the identity of dityrosine, authentic dityrosine standard was added to some samples and an increase in the intensity of the putative dityrosine band was observed (unpublished data).

Spectroscopic properties of di- and trityrosine

HPLC-purified samples of dityrosine and trityrosine from both *C. elegans* extracts and peroxidase domain cross-linking reactions were lyophilized and resolubilized in either 0.1 M HCl (3 ml) or 0.1 M NaOH (3 ml). Fluorescence excitation and emission spectra were obtained with a PerkinElmer LS-5B luminescence spectrometer.

Mass spectrometry

Mass spectrometry was preformed on a PerkinElmer sciex API 3000 triple quadruple mass spectrometer equipped with a turboionspray source. Dried dityrosine standard (20 mg) was reconstituted in 200 μl of H_2O. A 50-μl aliquot of this was diluted to a final volume of 1 ml with 950 μl of 5 mM ammonium acetate in MeOH and 1% acetic acid. This solution infused at a flow rate of 5 μl min^{-1}. The ionspray needle was held at +550 and −4500 V for positive and negative ion analysis, respectively. These experiments identified the singly protonated (positive ion mode) and deprotonated (negative ion mode) species of the standard to be *m/z* 361.3 and 359.3, respectively, corresponding to prediction.

Total protein, purified cuticle, and total protein minus purified cuticle acid hydrolysates from *C. elegans*, and standard were analyzed by reverse phase LC-MS/MS. A 50-μl volume of sample was injected onto a 15 cm × 2.1 mm Supelco Discovery C18 column at a flow rate of 300 μl min^{-1}. Solvent A was 99:1 H_2O to acetic acid and solvent B was 99:1 MeOHto acetic acid, both containing 5 mM ammonium acetate. The column was infused directly into the ion source of the mass spectrometer operating in positive ion mode. The column was preequilibrated with 100% solvent A for 6 min followed by sample injection. The column was then washed with 100% solvent A for 4 min and eluted with a 1 min linear gradient to 100% solvent B followed by a 4 min wash with 100% solvent B. For these experiments, both the precursor ions (as above for dityrosine; *m/z* 540.4/538.4 for trityrosine) and structurally distinctive breakdown ions were monitored. The transitions monitored for dityrosine were the neutral loss of both COOH groups, the neutral loss of both COOH groups and one NH_2 group, and the neutral loss of both COOH groups and both NH_2 groups (*m/z* 269.4, 252.2, and 235.0, respectively). For trityrosine, the transitions monitored were the neutral loss of a COOH group, the neutral loss of a COOH group and one NH_2 group, the neutral loss of two COOH-termini, and the neutral loss of two COOH groups and two NH_2 groups (*m/z* 494.3, 477.2, 448.2, and 431.2, respectively). *C. elegans* cuticle was purified according to methods developed previously by Cox et al. (1981).

Transmission electron microscopy

Approximately 120 wild-type or RNAi-blistered adult *C. elegans* were collected and washed first with M9 buffer and then with 0.1 M cacodylate buffer (pH 7.4). Animals were pelleted, added to 1 ml of 0.8% glutaraldeyde, 0.7% osmium tetroxide, 0.1 M cacodylate, pH 7.4, and incubated on ice for 1.5 h with occasional mixing. The animals were washed with 0.1 M cacodylate buffer, transferred to a glass depression slide, and cut in half with a 23-gauge needle. Bisected animals were transferred into a tube containing 1 ml of fresh fixative (0.8% glutaraldehyde, 0.7% osmium tetroxide, 0.1 M cacodylate, pH 7.4) and incubated on ice for 2 h. After washing with 0.1 M cacodylate buffer, the bisected animals were fixed overnight on ice in 1% osmium tetroxide in 0.1 M cacodylate buffer. Animals were washed several times in 0.1 M cacodylate buffer, dehydrated using graded alcohols through propylene oxide, infiltrated, and embedded in Embed-812 (Electron Microscopy Sciences). The animals were teased into parallel arrangement with an eyelash probe before polymerization at 60°C for 16 h. Sections (0.5 mm) were evaluated for orientation and ultrasections (800-Å thick) were collected on 200 mesh copper grids, stained with uranyl acetate and lead citrate, and cross sections were examined with a Philips EM201 electron microscope.

Construction of Duox peroxidase domain expression plasmids

The PCR was used to amplify the peroxidase domains of h-Duox (amino acid residues 1–593) and Ce-Duox (amino acid residues 1–590) from the cloned full-length sequences. The primers were designed to introduce an NH_2-terminal BamH I site and a COOH-terminal Not I site. PCR productsLL were digested with BamH I and Not I and ligated into the pET-32a(+) vector from Novogen. Plasmids were transformed into BL21(DE3) cells containing the chloramphenicol-resistant plasmid pT-groE (Yasukawa et al., 1995), which expresses the chaperonins groES and groEL from the T7 promoter. The pT-groE expression vector in BL21(DE3) cells was a gift from Dr. Lee-Ho Wang (University of Texas Health Science Center, Houston, TX) and Dr. Shunsuke Ishii (Institute of Physical and Chemical Research, Ibaraki, Japan). LB-agar plates containing both ampicillin and chloramphenicol were used to isolate colonies.

Expression of Duox peroxidase domains

A 0.5-ml LB overnight culture of cells containing plasmid with the peroxidase domain from h-Duox or Ce-Duox was used to inoculate 50 ml of modified TB medium (Sandhu et al., 1993) containing 0.5 mM δ-aminolevulinic acid, 100 μg/ml ampicillin, and 25 μg/ml chloramphenicol in a 250-ml flask. Bacteria were grown at 37°C in a shaker at 200 RPM until the cell density measured 0.7 OD at 600 nm. Isopropyl-β-D-thiogalactopyranoside (1 mM) was added, and the culture was continued at 25°C for 24 h at 150 RPM. Cells were pelleted at 4,500 *g* and resuspended in PBS containing 4-(2-aminoethyl)benzenesufnyl fluoride (2 μM), bestatin (130 nM), trans-epoxysuccinyl-L-leucyl-amido(4-guanidino)butane (1.4 nM), leupeptin (1 nM), and aprotinin (0.3 nM). The cell suspension was then sonicated on ice.

Activity assays

The TMB liquid substrate system (Sigma-Aldrich) was used to assay peroxidase activity (Holland et al., 1974). 100 μg of lysate protein from cells expressing either the human Duox1 peroxidase domain, Ce-Duox1 peroxidase domain, or a vector control was added to 1-ml aliquots of the TMB substrate system. The peroxidase reactions were performed in triplicate, and activity was monitored at 655 nm with a Beckman Coulter DU640B spectrophotometer. Some samples contained 30 μM aminobenzoic acid hydrazide, a peroxidase inhibitor (Kettle et al., 1995).

To assay tyrosine cross-linking, tyrosine ethyl ester (20 mM) was dissolved in 10 ml of PBS buffer supplemented with 80 μl of 3% H_2O_2. 100 μg of *E. coli* lysate protein was added to 1-ml aliquots, samples were incubated for 1 h, and the reaction was quenched using an equal volume of 12 M HCl. Samples were analyzed for di- and trityrosine as above.

We thank Robert Santoianni for carrying out the EM. Thanks also to Steve L'Hernault and Todd Lamitina for helpful advice and encouragement.

This research was supported by National Institutes of Health grants (CA84138 and AR/GM 44419). D.B. Flaherty is supported by a fellowship from the American Heart Association, Southeast Affiliate, and W.A. Edens is supported by a National Institutes of Health fellowship (DK 07298).

Submitted: 28 March 2001
Revised: 2 July 2001
Accepted: 3 July 2001

References

Abdelrahim, M., E. Morris, J. Carver, S. Facchina, A. White, and A. Verma. 1997. Liquid chromatographic assay of dityrosine in human cerebrospinal fluid. *J. Chromat. B. Biomed. Sci. App.* 696:175–182.

Anderson, S. 1963. Characterization of a new type of cross-linkage in resilin, a rubber-like protein. *Biochim. Biophys. Acta.* 69:249–262.

Babior, B.M. 1995. The respiratory burst oxidase. *Curr. Opin. Hematol.* 2:55–60.

Banfi, B., A. Maturana, S. Jaconi, S. Arnaudeau, T. Laforge, B. Sinha, E. Ligeti, N. Demaurex, and K.-H. Krause. 2000. A mammalian H^+ channel generated through alternative splicing of the NADPH oxidase homolog NOH-1. *Science.* 287:138–142.

Benian, G.M., T.L. Tinley, X. Tang, and M. Borodovsky. 1996. The *Caenorhabditis elegans* gene *unc*-89, required for muscle M-line assembly, encodes a giant modular protein composed of Ig and signal transduction domains. *J. Cell Biol.* 132:835–848.

Biberstine-Kinkade, B., L. Yu, and M. Dinauer. 1999. Mutagenesis of an arginine- and lysine-rich domain in the gp91^{phox} subunit of the phagocyte NADPH-oxidase flavocytochrome b_{558}. *J. Biol. Chem.* 274:10451–10457.

Briza, P., H. Kalchhauser, E. Pittenauer, G. Allmaier, and M. Breitenbach. 1996. N,N′-Bisformyl dityrosine is an in vivo precursor of the yeast ascospore wall. *Eur. J. Biochem.* 239:124–131.

Cheng, G., Z. Cao, X. Xu, E. van Mier, and J.D. Lambeth. 2001. Homologs of gp91*phox*: cloning and tissue expression of Nox3, Nox4 and Nox5. *Gene.* 269:131–140.

Clark, R.A., S. Szot, M.A. Williams, and H.M. Kagan. 1986. Oxidation of lysine side-chains of elastin by the myeloperoxidase system and by stimulated human neutrophils. *Biochem. Biophys. Res. Commun.* 135:451–457.

Cox, G.N., M. Kusch, and R.S. Edgar. 1981. Cuticle of the *Caenorhabditis elegans*: its isolation and partial characterization. *J. Cell Biol.* 90:7–17.

Cross, A.R., and O.T.G. Jones. 1991. Enzymic mechanisms of superoxide production. *Biochim. Biophys. Acta.* 1057:281–298.

Cross, A., J. Rae, and J. Curnutte. 1995. Cytochrome b_{-245} of the neutrophil superoxide-generating system contains two nonidentical hemes. *J. Biol. Chem.*

270:17075–17077.

De Deken, X., D. Wang, M.-C. Many, S. Costagliola, F. Libert, G. Vassart, J.E. Dumont, and F. Miot. 2000. Cloning of two human thyroid cDNAs encoding new members of the NADPH oxidase family. *J. Biol. Chem.* 227:23227–23233.

Deits, T., M. Farrance, E. Kay, L. Medill, E. Turner, P. Weidman, and B. Shapiro. 1984. Purification and properties of ovoperoxidase, the enzyme responsible for hardening the fertilization membrane of the sea urchin egg. *J. Biol. Chem.* 259:13525–13533.

Dupuy, C., R. Ohayon, A. Valent, M. Noe-Hudson, D. Dee, and A. Virion. 1999. Purification of a novel flavoprotein involved in the thyroid NADPH-oxidase. *J. Biol. Chem.* 274:37265–37269.

Emmendorffer, A., J. Roesler, J. Elsner, E. Raeder, M.-L. Lohmann-Matthes, and B. Meier. 1993. Production of oxygen radicals by fibroblasts and neutrophils from a patient with x-linked chronic granulomatous disease. *Eur. J. Haematol.* 51:223–227.

Fetterer, R., and M. Rhoads. 1990. Tyrosine-derived cross-linking amino acids in the sheath of *haemonchus contortus* infective larvae. *J. Parasitol.* 76:619–624.

Fetterer, R., M. Rhoads, and J. Urban. 1993. Synthesis of tyrosine-derived cross-links in *ascaris suum* cuticular proteins. *J. Parasitol.* 79:160–166.

Fire, A., S. Xu, M.K. Montgomery, S.A. Kostas, S.E. Driver, and C.C. Mellow. 1998. Potent and specific genetic interference by double-stranded RNA in *Caenorhabditis elegans*. *Nature.* 391:806–811.

Francis, R., and R.H. Waterston. 1991. Muscle cell attachment in *C. elegans*. *J. Cell Biol.* 114:465–479.

Garcia-Castineiras, S., J. Dillon, and A. Spector. 1978. Non-tryptophan fluorescence associated with human lens protein; apparent complexity and isolation of bityrosine and anthranilic acid. *Exp. Eye Res.* 26:461–476.

Georgi, F., and P. Deri. 1976. Cytochemistry of late ovarian chambers of *Drosophila melanogaster*. *Histochem*. 48:325–334.

Griendling, K., C. Minieri, J. Ollerenshaw, and R. Alexander. 1994. Angiotensin II stimulates NADH and NADPH-oxidase activity in cultured vascular smooth muscle cells. *Circ. Res.* 74:1141–1148.

Grupta, M.C., P.L. Graham, J.M. Kramer. 1997. Characterization of α1(IV) collagen mutations in *Caenorhabditis elegans* and the effects of α1 α2(IV) mutations on type IV collagen distribution. *J. Cell Biol.* 137:1185–1196.

Hall, H.G. 1978. Hardening of the sea urchin fertilization envelope by peroxidase catalyzed phenolic coupling of tyrosines. *Cell.* 15:343–355.

Hampton, M.B., A.J. Kettle, and C.C. Winterbourn. 1998. Inside the phagosome: oxidants, myeloperoxidase and bacterial killing. *Blood.* 92:3007–3017.

Hazen, S.L., J.P. Gaut, F.F. Hsu, J.R. Crowley, A. d'Avingnon, and J.W. Heinecke. 1997. p-Hydroxyphenylacetaldehyde, the major product of L-tyrosine oxidation by the myeloperoxidase-H_2O_2-chloride system of phagocytes, covalently modifies ϵ-amino groups of protein lysine residues. *J. Biol. Chem.* 272:16990–16998.

Heinecke, J., W. Li, H. Daehnke, and J. Goldstein. 1993. Dityrosine, a specific marker of oxidation, is synthesized by the myeloperoxidase-hydrogen peroxide system of human neutrophils and macrophages. *J. Biol. Chem.* 268: 4069–4077.

Hill, A.A., C.P. Hunter, B.T. Tsung, G. Tucker-Kellogg, and E.L. Brown. 2000. Genomic analysis of gene expression in *C. elegans*. *Science*. 290:809–812.

Holland, V.R., B.C. Saunders, F.L. Rose, and A.L. Walpole. 1974. A safer substitute for benzidine in the detection of blood. *Tetrahedron.* 30:3299–3302.

Jacob, J.S., D.P. Cistola, F.F. Hsu, S. Muzaffar, D.M. Mueller, S.L. Hazen, and J.W. Heinecke. 1996. Human phagocytes employ the myeloperoxidase-hydrogen peroxide system to synthesize dityrosine, trityrosine, pulcherosine, and isodityrosine by a tyrosyl radical-dependent pathway. *J. Biol. Chem.* 271:19950–19956.

Johnstone, I. 2000. Cuticle collagen genes expression in *Caenorhabditis* elegans. *Trends Genet.* 16:21–27.

Keeley, F.W., F. LaBella, and G. Queen. 1969. Dityrosine in a non-hydroxyproline, alkali-soluble protein isolated from chick aorta and bovine ligament. *Biochem. Biophys. Res. Commun.* 34:156–161.

Kettle, A.J., C.A. Gedye, M.B. Hampton, and C.C. Winterbourn. 1995. Inhibition of myeloperoxidase by benzoic acid hydrazides. *Biochem. J.* 308:559–563.

Klebanoff, S., C. Foerder, E. Eddy, and B. Shapiro. 1979. Metabolic similarities between fertilization and phagocytosis. *J. Exp. Med.* 149:938–953.

LaBella, F., F. Kesley, S. Vivian, and D. Thornhill. 1967. Evidence for dityrosine in elastin. *Biochem. Biophys. Res. Comm.* 26:748–753.

LaBella, F., P. Waykole, and G. Queen. 1968. Formation of insoluble gels and dityrosine by the action of peroxidase on soluble collagens. *Biochem. Biophys. Res. Comm.* 30:333–338.

Lambeth, J.D., G. Cheng, R.S. Arnold, and W.A. Edens. 2000. Novel homologs of gp91*phox*. *Trends Biochem. Sci.* 25:459–461.

Leeuwenburgh, C., J. Rasmussen, F. Hsu, D. Mueller, S. Pennathur, and J. Heinecke. 1997. Mass spectrometric quantification of markers for protein oxidation by tyrosyl radical, copper, and hydroxyl radical in low density lipoprotein isolated from human atherosclerotic plaques. *J. Biol. Chem.* 272: 3520–3526.

Levy, D., J. Yang, and M. Kramer. 1993. Molecular and genetic analysis of the *Caenorhabditis elegans* dpy-2 and dpy-10 collagen genes: a variety of molecular alterations affect organismal morphology. *Mol. Biol. Cell.* 4:803–817.

Locke, M. 1969. The localization of a peroxidase associated with hard cuticle formation in an insect, *Calpodes Ethlius* Stoll, Lepidoptera, Hesperiidae. *Tissue Cell.* 1:555–574.

Malanik, V., and M. Ledvina. 1979. Preparation and isolation of dityrosine. *Prep. Biochem.* 9:273–280.

Miller, D.M., I. Ortiz, G.C. Berliner, and H.F. Epstein. 1983. Differential localization of two myosins within nematode thick filaments. *Cell.* 34:477–490.

Mindrinos, M.N., W.H. Petri, V.K. Galanopoulos, M.F. Lombard, and L.H. Margaritis. 1980. Crosslinking of the *Drosophila* chorion involves a peroxidase. *Wilhelm Roux's Arch. Dev. Biol.* 189:187–196.

Nauseef, W. 1998. Insights into myeloperoxidase biosynthesis from its inherited deficiency. *J. Mol. Med.* 76:661–668.

Nielsen, H., J. Engelbrecht, S. Brunak, and G. von Heijne. 1997. Identification of prokaryotic and eukaryotic signal peptides and prediction of their cleavage sites. *Protein Eng.* 10:1–6.

Nisimoto, Y., H. Otsuka-Murakami, and J.D. Lambeth. 1995. Reconstitution of flavin-depleted neutrophil flavocytochrome b_{558} with 8-Mercapto-FAD and characterization of the flavin-reconstituted enzyme. *J. Biol. Chem.* 270: 16428–16434.

Raven, D.J., C. Earland, and M. Little. 1971. Occurrence of dityrosine in Tussah silk fibroin and keratin. *Biochim. Biophys. Acta.* 251:96–99.

Rotrosen, D., C.L. Yeung, T.L. Leto, H.L. Malech, and C.H. Kwong. 1992. Cytochrome b_{558}: the flavin-binding component of the phagocyte NADPH-oxidase. *Science.* 256:1459–1462.

Sandhu, P., T. Baba, and F.P. Guengerich. 1993. Expression of modified cytochrome P450 2C10 (2C9) in *Escherichia coli*, purification and reconstitution of catalytic activity. *Arch. Biochem. Biophys.* 312:443–450.

Segal, A.W., I. West, F. Wientjes, J.H.A. Nugent, A.J. Chavan, B. Haley, R.C. Garcia, H. Rosen, and G. Scrace. 1992. Cytochrome b^{-245} is a flavocytochrome containing FAD and the NADPH-binding site of the microbicidal oxidase of phagoctyes. *Biochem. J.* 284:781–788.

Sonnhammer, E., G. von Heijne, and A. Krogh. 1998. Proceedings of the Sixth International Conference on Intelligent Systems for Molecular Biology. J. Glasgow, F. Littlejohn, R. Major, R. Lathrop, D. Sankoff, and C. Sensen, editors. AAAI Press, Menlo Park, CA. 175–182.

Stahmann, M.A., A.K. Spencer, and G.A. Honold. 1977. Cross linking of proteins in vitro by peroxidase. *Biopolymers*. 16:1307–1318.

Suh, Y.-A., R.S. Arnold, B. Lassegue, J. Shi, X. Xu, D. Sorescu, A.B. Chung, K.K. Griendling, and J.D. Lambeth. 1999. Cell transformation by the superoxide-generating oxidase Mox1. *Nature.* 401:79–82.

Sumimoto, H., N. Sakamoto, M. Nozaki, Y. Sakaki, K. Takeshige, and S. Minakami. 1992. Cytochrome b558, a component of the phagocyte NADPH-oxidase, is a flavoprotein. *Biochem. Biophys. Res. Commun.* 186:1368–1375.

Takeshige, K., and H. Sumimoto. 1994. Cytochrome b_{558}: a flavocytochrome comprising the complete electron-transporting apparatus of phagocyte NADPH-oxidase. *In* Regulation of Heme Protein Synthesis. 97–102 pp.

Taurog, A. 1999. Molecular evolution of thyroid peroxidase. *Biochimie.* 81:557–582.

Taylor, W.R., D.T. Jones, and A. Segal. 1993. A structural model for the nucleotide binding domains of the flavocytochrome b_{-245} β-chain. *Protein. Sci.* 2:1675–1685.

Tenovuo, J., and K. Paunio. 1979. Formation of dityrosine by human salivary lactoperoxidase in vitro. *Acta Odontol. Scand.* 37:147–152.

Wallach, T.M., and A.W. Segal. 1997. Analysis of glycosylation sites on gp91phox, the flavocytochrome of the NADPH-oxidase, by site-directed mutagenesis and translation in vitro. *Biochem. J.* 321:583–585.

Waykole, P., and E. Heidemann. 1976. Dityrosine in collagen. *Connect Tissue Res.* 4:219–222.

Winterbourn, C.C., M.C. Vissers, and A.J. Kettle. 2000. Myeloperoxidase. *Curr. Opin. Hematol.* 7:53–58.

Yasukawa, T., C. Kanei-Ishii, T. Maekawa, J. Fujimoto, T. Yamamoto, and S. Ishii. 1995. Increase of solubility of foreign proteins in *Escherichia coli* by coproduction of the bacterial thioredoxin. *J. Biol. Chem.* 270:25328–25331.

Yu, L., M.T. Quinn, A.R. Cross, and M.C. Dinauer. 1998. Gp91(phox) is the heme binding subunit of the superoxide-generating NADPH-oxidase. *Proc. Natl. Acad. Sci. USA.* 95:7993–7998.

Zaitsu, K., S. Eto, and Y. Ohkura. 1981. High-performance liquid chromatographic determination of dityrosine in biological samples. *J. Chromatogr.* 206:621–624.

Zeng, J., and R.E. Fenna. 1992. X-ray crystal structure of canine myeloperoxidase at 3 Å resolution. *J. Mol. Biol.* 226:185–207.